THE JOURNAL OF PHYSICAL CHEMISTRY C

Article

pubs.acs.org/JPCC

Sulfurization-Assisted Cobalt Deposition on $Sm_2Ti_2S_2O_5$ Photocatalyst for Water Oxidation under Visible Light Irradiation

Rengui Li,[†,‡] Zheng Chen,[†,‡] Wen Zhao,[§] Fuxiang Zhang,[†] Kazuhiko Maeda,[§,∥] Baokun Huang,[†] Shuai Shen,[†,‡] Kazunari Domen,*[,§] and Can Li*[,†]

[†]State Key Laboratory of Catalysis, Dalian National Laboratory for Clean Energy, Dalian Institute of Chemical Physics, Chinese Academy of Sciences, Zhongshan Road 457, Dalian 116023, China

[‡]Graduate University of Chinese Academy of Sciences, Beijing 100049, China

[§]Department of Chemical System Engineering, the University of Tokyo, 7-3-1 Hongo, Bunkyo-ku, Tokyo 113-8656, Japan

[∥]Precursory Research for Embryonic Science and Technology (PRESTO), Japan Science and Technology Agency (JST), 4-1-8 Honcho Kawaguchi, Saitama 332-0012, Japan

Supporting Information

ABSTRACT: Deposition of cocatalyst is an efficient way for photocatalytic water splitting to improve solar energy conversion efficiency, and its deposition method has been known to make a great effect. In this work, we introduced a sulfurization-assisted deposition method to load earth-abundant cobalt cocatalyst for the purpose of promoting water oxidation performance of $Sm_2Ti_2S_2O_5$ oxysulfide that is characterized with wide visible light absorption. The cobalt deposition introduced here undergoes first formation of CoS_x by sulfurization at high temperature and subsequent conversion into CoO_x by calcinations in air. Compared to conventionally impregnated cobalt or IrO_2 colloids, the sulfurization-assisted cobalt deposition well maintains structure of photocatalyst and inhibits the formation of defect sites leading to better separation of photogenerated carriers and water oxidation performance. The apparent quantum efficiency of the optimized sample reaches 5.0% at 420 nm. The sulfurization-assisted deposition actually open a new way to modify the (oxy)sulfide semiconductors.

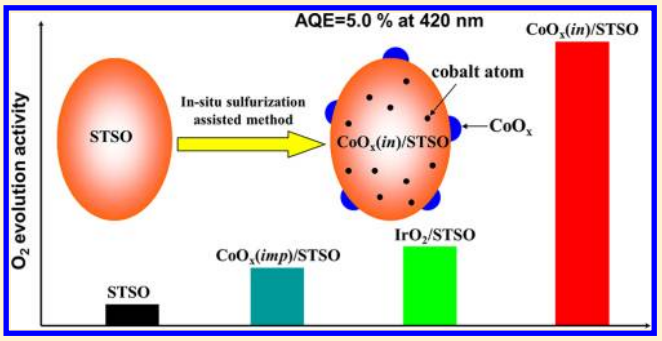

INTRODUCTION

Semiconductor-based powder photocatalyst for water splitting or reduction of CO_2 is regarded as one of the ideal ways to convert solar energy into chemical energy,[1−4] among which water oxidation process is the key challenging step.[5,6] To achieve efficient water oxidation, loading of active oxidation cocatalyst is necessary. Structures and chemical states of the cocatalyst are very important factors affecting the water oxidation performance and both of which are greatly related to the loading way of the cocatalyst onto the semiconductor.[7,8] Thus, it is desirable to develop effective deposition method and/or processes to control the local structure of the deposited cocatalysts.

Some noble metal oxides such as RuO_2[9−12] and IrO_2[13−16] have been found to be efficient O_2 evolution cocatalysts in many photocatalytic systems, but efficient cocatalysts composed of only earth-abundant elements are still limited. Recently, cobalt-based cocatalysts such as CoPi,[17−19] $NiCo_2O_4$,[20,21] and CoO_x[22−24] have been reported to be active for photo(electro)-chemical water splitting, showing potential to replace noble metal oxides, and various preparation methods have been reported.

Some (oxy)nitrides and oxysulfides have been developed as potential water splitting materials with wide visible light absorption.[14,23,25−30] In order to improve water oxidation activity of these materials, a series of metal oxides have been deposited as oxidation cocatalysts by impregnation or absorption methods.[31−34] Oxysulfide $Sm_2Ti_2S_2O_5$ (STSO) is a kind of visible light-driven photocatalysts with a band gap of 2.0 eV and shows stable photocatalytic H_2 or O_2 evolution in the presence of sacrificial reagents.[27,28,35] Although IrO_2 colloidal was found to be the best water oxidation cocatalysts on it, its photocatalytic water oxidation activity is still low.[27,28]

Herein, we will introduce a novel sulfurization-assisted deposition method for loading cobalt oxide as cocatalyst on $Sm_2Ti_2S_2O_5$ oxysulfide. Different from conventional impregnation process, the cobalt deposition in this work undergoes the formation of CoS_x by sulfurization at high temperature and subsequent conversion into CoO_x by calcination in air. Compared to conventionally impregnated cobalt oxide or

Received: October 14, 2012
Revised: December 13, 2012
Published: December 17, 2012

   dx.doi.org/10.1021/jp310138b | J. Phys. Chem. C 2013, 117, 376−382

IrO_2 colloids, the sulfurization-assisted cobalt deposition shows much higher water oxidation performance. After the optimization of the cobalt content and deposition way, the photocatalytic O_2 evolution activity of $CoO_x(in)$/STSO can be enhanced by about 16 times of the parent STSO photocatalyst and 6 times of $CoO_x(imp)$/STSO, which was prepared by traditional impregnation method. The apparent quantum efficiency of $CoO_x(in)$/STSO in the first hour irradiation is measured at 5.0% at 420 nm, which is the highest O_2 evolution efficiency for oxysulfides reported so far.

EXPERIMENTAL SECTION

Preparation of Photocatalysts. The synthesis of $Sm_2Ti_2S_2O_5$ is similar to that in previous report.[35−37] Generally, it involves two steps: (i) synthesis of an amorphous oxide precursor by a polymerized complex method and (ii) sulfurization of the oxide precursor under an H_2S flow. The oxide precursor was synthesized by the polymerized complex (PC) method with typical processes as follows: 0.02 mol of titanium tetraisopropoxide (Kanto Chemicals Co., Purity 98.0%) was dissolved in 0.2 mol of ethylene glycol (Kanto Chemicals Co., Purity 99.0%) at room temperature, and 0.3 mol of anhydrous citric acid (Wako Pure Chemicals, Purity 99.5%) was then added and the mixture was heated at 333 K until it was completely dissolved. Subsequently, 0.02 mol of $Sm(NO_3)_3{\cdot}6H_2O$ (Kanto Chemicals Co., purity 99.0%) and 20 mL of methanol were added to the solution in that order. The mixture was stirred at 403 K until a transparent gel was formed. The polymer was carbonized at temperatures of 573 K for 1 h and finally annealed at 773 K for 12 h to completely remove the carbon. The as-prepared samples were denoted as "STO". The STO precursor was sulfurized at 1223 K for 1 h under a flow of H_2S (10 mL/min). Postcalcination for 2 h in air at 573 K was then carried out to remove any sulfur species adsorbed on the surface of the photocatalyst. The as-prepared sample is denoted as "STSO". Similarly, 2 wt % cobalt doped STSO sample was also prepared for comparison. Meanwhile, the cobalt nitrate as precursor will be added once the transparent gel was formed during the synthesis of STO.

Deposition of Cocatalysts. Cobalt oxide as cocatalyst was deposited under the assistance of sulfurization by two different routes: one is called *in situ*, and the other is *ex situ*. The *in situ* cobalt deposition was achieved simultaneously as the synthesis of $Sm_2Ti_2S_2O_5$ (STSO). Typically, $Sm_2Ti_2O_7$ (STO) was prepared by the PC method, on which a different amount of cobalt nitrate was impregnated. Subsequently, the cobalt impregnated STO (Co-STO) was sulfurized at 1223 K for 1 h under the flow of H_2S (10 mL/min). Postcalcinations in air at 573 K for 1 h were then carried out to convert surface cobalt species into oxide. The as-achieved sample is denoted as $CoO_x(in)$/STSO. As for the *ex situ* cobalt deposition, STSO powder was first prepared by sulfurizing the STO precursor as above-described, and a calculated amount of cobalt nitrate was then impregnated onto its surface. The impregnated powder was further transferred into a quartz tube for sulfurization under the flow of H_2S at 773−1073 K for 1 h. The as-sulfurized powder was annealed in air at 373−673 K for 1 h. In this work, the temperature effect of the sulfurization and calcinations was evaluated by the water oxidation performance, and the optimal values are 973 and 573 K, respectively, which are therefore used in this work if it is not specially stated. The as-achieved sample is denoted as $CoO_x(ex)$/STSO. As a comparison, cobalt oxide was also deposited by conventional impregnation method, and the optimal cobalt content was also examined as 2 wt %. The photocatalyst is here remarked as $CoO_x(imp)$/STSO. In addition, IrO_2 colloid with optimized content of 2 wt % was adsorbed on the surface of STSO as cocatalyst, and the catalyst is denoted as IrO_2/STSO. If it is not specially stated, the content of the cocatalyst in this work are all calculated by the metal weight.

Preparation of Photoelectrodes. The STSO and $CoO_x(in)$/STSO film electrodes (1 × 1 cm^2) were prepared on FTO substrate by electrophoretic deposition. Typically, the electrophoretic deposition was carried out in an acetone solution (75 mL) containing powder samples (100 mg) and iodine (20 mg), which was dispersed by sonication for 15 min. The FTO electrode was immersed, parallel with the Pt electrode, the distance between two electrode was 5 cm, and 20 V of bias was applied for 1 min using a potentiostat (ITECH IT6834). The electrode was dried and then calcined at 573 K for 1 h.

Photocatalytic Reactions for Water Oxidation. The photocatalytic water oxidation performances were performed with a Pyrex reactor at room temperature and carried out in a closed gas circulation and evacuation system using a 300 W Xe lamp (Ushio-CERMAXLX300) and optical cutoff filter (Kenko, L-42; $\lambda \geq 420$ nm). Normally, 0.10 g of photocatalyst was dispersed in 150 mL of 0.02 M aqueous $AgNO_3$ solution in a Pyrex reaction cell and thoroughly degassed by evacuation in order to drive off the air inside. 0.20 g of La_2O_3 was used to adjust the pH value to 8.5.[27,28] The amount of evolved O_2 was determined by an online gas chromatograph (Agilent, GC-7890, TCD, Ar carrier). The amount of O_2 evolved in the first hour was measured to evaluate the photocatalytic activity of the samples.

Photoelectrochemical Measurements. Photoelectrochemical performances of STSO and $CoO_x(in)$/STSO electrodes were measured in a three-electrode setup in a 0.1 M NaOH solution (pH = 13.0). The counter electrode was Pt electrode, and the reference electrode was saturation mercury electrode (SCE). For linear sweep voltammetry, the potential was swept with scan rate of 10 mV/s. A 300 W Xe lamp (CERMAX, LX300) and optical cutoff filter (Kenko, L-42; $\lambda \geq 420$ nm) were used as light source.

Quantum Efficiency Measurement. The apparent quantum efficiency (AQE) was measured using a Pyrex top-irradiation-type reaction vessel and a 300 W xenon lamp fitted with a 420 nm band-pass filter. Photocatalytic water oxidation was examined using an aqueous solution (150 mL) containing 0.20 g of CoO_x (in)/STSO, 0.20 g of La_2O_3, and 0.01 M $AgNO_3$ reagents. The number of photons reaching the solution was measured with a Si photodiode. Quantum efficiency (Φ) values were calculated using the equation

$$\Phi\ (\%) = (AR/I) \times 100\%$$

where A, R, and I represent the coefficients (4 for O_2 evolution), the O_2 evolution rate (mol h^{-1}), and the rate of absorption of incident photons, respectively. Here, Φ is the apparent quantum efficiency because we assume that all incident photons are absorbed by the suspension.

Characterization of Catalyst. The existing states of the deposited cobalt were characterized by X-ray photoelectron spectroscopy (XPS) measurements, using a VG ESCALAB MK2 spectrometer with monochromatized Al Kα excitation. The binding energy (284.6 eV) of the C 1s peak was used as reference. A Raman spectrum was carried out on Renisha-

dx.doi.org/10.1021/jp310138b | J. Phys. Chem. C 2013, 117, 376−382

Scheme 1. Specific Experiment for the *in Situ* and *ex Situ* Cobalt Deposition

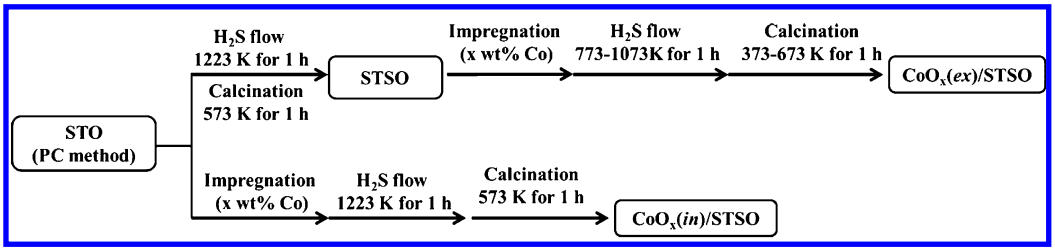

winVia Raman microscope. High-resolution TEM (HRTEM) micrographs were taken on a JEM-2000eX transmission electron microscope. X-ray powder diffraction (XRD) was carried out on a Rigaku D/Max-2500/PC powder diffractometer. The sample powder was scanned using Cu Kα radiation with an operating voltage of 40 kV and an operating current of 200 mA. The scan rate of 5°/min was applied to record the patterns in the range of 10°−80° at a step size of 0.02°. Photoluminescence spectroscopy was measured at 77 K under 400 nm excitation using an FP-6600 instrument (Jasco). The transient IR absorption signals were recorded on the Nicolet 870 FTIR spectrometer with the MCT detector. The pulse laser at 355 nm (1 Hz, 3 mJ/pulse) was used to excite the samples. The wavelength of the detection of IR absorption is from 1000 to 4000 cm^{-1}. The synchronization between laser excitation and data acquisition was achieved with a Stanford Research Model DG535 pulse generator.

RESULTS AND DISCUSSION

In order to well understand the sulfurization-assisted cobalt deposition effect, two experimental procedures were used and compared, which are called here as "*in situ*" and "*ex situ*" cobalt deposition process, respectively. The as-prepared samples are correspondingly denoted as $CoO_x(in)$/STSO and $CoO_x(ex)$/STSO, respectively. The cobalt deposition processes are summarized in Scheme 1. The difference of the *in situ* and *ex situ* cobalt deposition processes lies in the cobalt deposition achieved during or after the preparation of STSO.

Figures 1a and 1b show the XRD patterns and UV−vis spectra of STSO separately, from which single phase of well-crystallized STSO particles with absorption edge of about 600 nm can be demonstrated. Compared to the XRD diffraction peaks of the parent STSO, similar patterns and widths are observed for the cobalt-modified STSO samples shown in Figure 1c, demonstrating the oxysulfide structure is kept after the cobalt modification. In the magnified view of XRD patterns (Figure 1d), however, the diffraction peak of the $CoO_x(in)$/STSO sample is slightly shifted to higher degree by 0.1° with respect to STSO, demonstrating that the cobalt atoms are partially incorporated into the crystal lattice of STSO to replace Ti atoms. In consideration of the similarity of ion radii between Ti^{4+} and Co^{2+} (Ti^{4+}: 74.5 pm; Co^{2+}: 74.0 pm; Co^{3+}: 68.5 pm; and Co^{4+}: 67.0 pm), the obvious diffraction shift is proposed to result from the substitution of Ti^{4+} by cobalt ions with higher valences such as Co^{3+} or Co^{4+}. It should be mentioned that the coordination numbers of Sm^{3+} and Ti^{4+} ions in STSO are 12 and 6, respectively, and it is difficult for cobalt ions to have 12-coordinated state, so the substitution of cobalt to samarium atoms is impossible. The substitution of Co to Ti atoms is further confirmed by the similar diffraction shift in the XRD patterns of Co-doped STSO photocatalyst that was prepared by sulfurizing Co-doped STO (PC method) sample. The *ex situ* cobalt deposition does not cause obvious shift of diffraction, demonstrating its little or no cobalt doping. No additional peaks associated with cobalt additives are observed for all the samples presumably owing to the low content of the deposited cobalt.

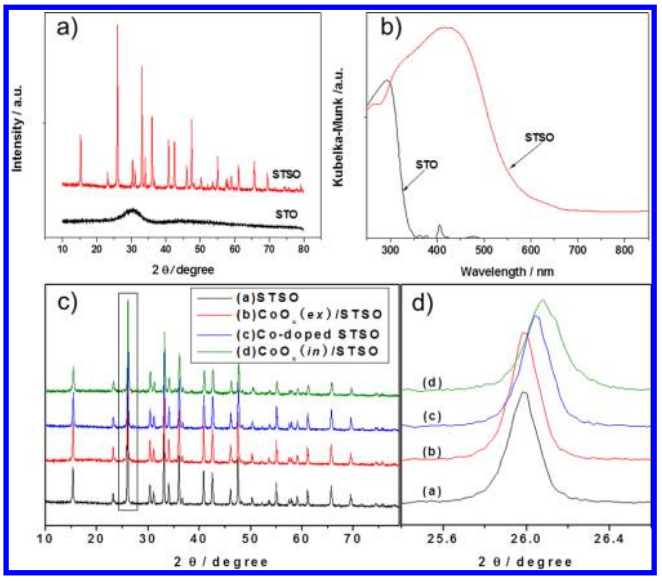

Figure 1. Various characterizations of STSO and cobalt-modified STSO samples: (a) XRD patterns; (b) UV−vis spectra; (c, d) XRD patterns of the STSO samples: (a) STSO, (b) $CoO_x(ex)$/STSO, (c) Co-doped STSO, (d) $CoO_x(in)$/STSO.

The formation of cobalt oxide on the surface of STSO sample was determined by high-resolution TEM (HRTEM), XPS spectroscopy, and Raman spectroscopy. The cobalt oxide nanoparticles on the surface of STSO powder are directly observed by the HRTEM micrograph in Figure 2, where the lattice spaces of the fringes (d = 0.206, 0.237, or 0.287 nm) well correspond to the (400), (222), and (200) crystal facets of Co_3O_4, respectively. It should be mentioned that some CoO oxides (d = 0.215 or 0.222 nm) and aggregated cobalt oxides are also observed (Figure S1). For simplicity, the deposited cobalt is thus described as CoO_x. Typical XPS spectra show that the binding energies of Co $2p_{3/2}$ and Co $2p_{1/2}$ peaks are located at 780.9 and 786.9 eV, respectively (Figure S2), which are in good accordance with the positions of both $Co^{2+}$and Co^{3+} reported in the literature,[23,38,39] and the satellite peak at 787.5 eV is a characteristic feature of Co(II) ions. In addition, the formation of cobalt oxide is further evidenced by the Raman spectrum of $CoO_x(in)$/STSO together with the parent STSO, Co_3O_4, and Co_3S_4 samples as references shown in Figure 3, where the Raman band at 691 cm^{-1} is ascribed to the Co_3O_4.[40]

To better understand the formation process of cobalt oxide, the conversion of cobalt precursor $Co(NO_3)_2$ without addition of STSO photocatalyst was examined by a similar procedure to

dx.doi.org/10.1021/jp310138b | J. Phys. Chem. C 2013, 117, 376−382

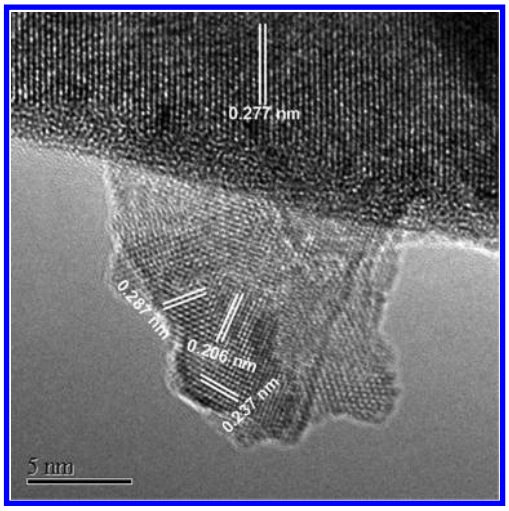

Figure 2. High-resolution TEM image of $CoO_x(in)$/STSO.

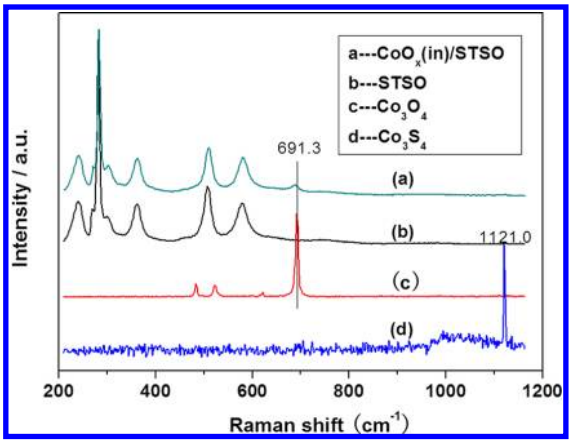

Figure 3. Raman spectra of $CoO_x(in)$/STSO, STSO, Co_3O_4, and Co_3S_4 samples as references.

the *ex situ* cobalt deposition. As indicated by the XRD patterns and Raman spectra (Figure S3), cobalt oxide Co_3O_4 was initially formed owing to thermal decomposition of cobalt nitrate at high temperature annealing and which will be converted into CoS_x (Co_3S_4 and rare CoS, denoted as CoS_x) after the sulfurization at 1023 K under the flow of H_2S. Afterward, the formed CoS_x is transformed into Co_3O_4 oxide again after postcalcination in air at 573 K. It is therefore reasonable to deduce that the formation of CoO_x oxide on the $CoO_x(in)$/STSO photocatalyst undergoes first decomposition of cobalt nitrate into Co_3O_4 and subsequent sulfurization to form CoS_x which was finally oxidized into CoO_x.

Table 1 compares photocatalytic water oxidation performances of STSO samples without and with different cocatalysts under visible light irradiation in the presence of $AgNO_3$ as electron acceptor. The parent STSO sample shows very low photocatalytic O_2 activity, while the *in situ* and *ex situ* cobalt deposition lead to obvious enhancement of O_2 evolution activity, demonstrating clear promotion effect on the O_2 evolution activity. It is interesting to note that the promotion effect is strongly dependent on the amount of loaded cobalt, and the optimal cobalt loading values are 2 and 1 wt % for the *in situ* and *ex situ* cobalt deposition, respectively (Figure S4). The maximal activity of O_2 evolution (163 μmol/h) is achieved by the *in situ* cobalt deposition, which is about 16 times that of

Table 1. Influence of Cocatalysts on the O_2 Evolution of STSO Photocatalyst[a]

entry	cocatalyst	O_2 evolution rate (μmol/h)
1	none	10
2	2 wt % $CoO_x(in)$	163
3	1 wt % $CoO_x(ex)$	65
4	2 wt % $CoO_x(imp)$	29
5	2 wt % IrO_2	46
6	2 wt % Co-doped	38

[a]Reaction conditions: catalyst, 0.10 g (0.20 g of La_2O_3 as a buffer); reaction solution, aqueous silver nitrate solution (0.02 M, 150 mL); light source, xenon lamp (300 W) with cutoff filter; reaction vessel, top-irradiation type; 1 h irradiation.

the parent STSO sample. Similarly, the conventionally impregnated cobalt or adsorption of IrO_2 colloids can improve the photocatalytic water oxidation performance, but the promotion effect is not as evident as the sulfurization-assisted sample here, especially for the *in situ* process. In addition, the Co-doped STSO photocatalyst shows higher water oxidation performance than the parent STSO one, indicating availability of cobalt ion doping in promoting water oxidation. It should be pointed out that the CoO_x itself does not work for water oxidation even in the $AgNO_3$-containing aqueous solution with or without light irradiation. The apparent quantum efficiency on the 2 wt % $CoO_x(in)$/STSO sample was measured as 5.0% at 420 nm. To the best of our knowledge, this is the highest O_2 evolution efficiency achieved on the oxysulfides.

Time course of O_2 evolution on the $CoO_x(in)$/STSO sample was shown to evaluate the stability of photocatalyst (Figure S5). No reaction took place in the dark, and the gas evolution began with the onset of light. The rate of O_2 evolution decreased with the increasing reaction time because the photocatalyst was covered with the reduced metal Ag, hindering light absorption and decreasing the number of active sites available. Similar experimental phenomena have been reported in previous references using $AgNO_3$ as the electron scavenger.[23,41−44] No obvious changes in the XRD patterns (not given) were observed for the $CoO_x(in)$/STSO samples before and after reactions except that some new peaks assigned to La_2O_3 added appear in the sample after reaction, indicating good stability of our sample. Similar stability of the photocatalyst was observed in previous reports.[27,28]

To know about the promotion effect of the deposited cobalt on the water oxidation, several experiments were performed. The photoelectrochemical performance of the STSO and cobalt-modified STSO electrodes are compared. The cobalt-modified STSO electrode gives a much higher anodic photocurrent upon visible light irradiation and a more negative photocurrent onset potential with respect to the bare STSO electrode (Figure 4). This indicates that CoO_x deposited on the surface of STSO does indeed promote the water oxidation as an efficient cocatalyst. Another reference experiment also indicates that when the cobalt-modified STSO sample was not subject to postcalcination in air, the photocatalyst shows almost the same O_2 evolution activity as bare STSO, indicating that CoS_x is not efficient for O_2 evolution. The photocatalytic activity of different samples with different calcination temperature was also be examined (Figure S6). As the calcination temperature increased, the higher O_2 evolution activity was obtained, and at 573 K, it reached the best performance. With further increase of temperature, the activity was decreased, which may due to the

dx.doi.org/10.1021/jp310138b | J. Phys. Chem. C 2013, 117, 376−382

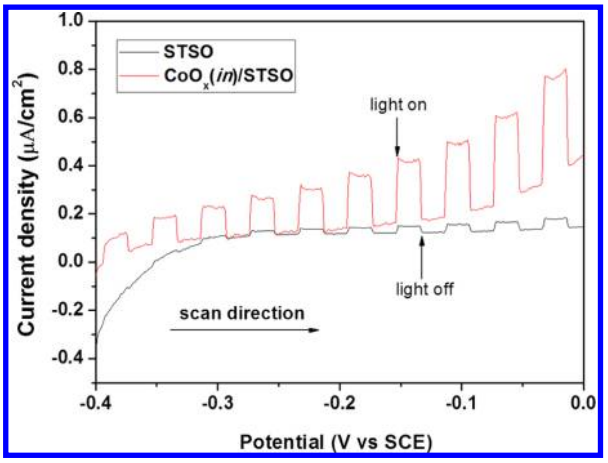

Figure 4. Photoanode currents of STSO electrodes with and without cobalt loading in 0.1 M NaOH aqueous solution (pH = 13.0). Scan rate: 10 mV s^{-1}.

oxidative degradation of the oxysulfide structure (Figure S7). This result indicates that the conversion of CoS_x into CoO_x in the step 3 is necessary for the water oxidation. That is to say, the CoO_x, not CoS_x, is the active cocatalyst for water oxidation. Compared to the bare STSO powder, the surface area of the $CoO_x(in)$/STSO sample is slightly decreased from 6.0 to 5.4 m^2/g, demonstrating its unfavorable contribution to water oxidation performance (Table S1).

Photoluminescence (PL) spectra were used to further examine the influence of cobalt doping and/or deposition on the structure of the photocatalysts (Figure 5). The unmodified

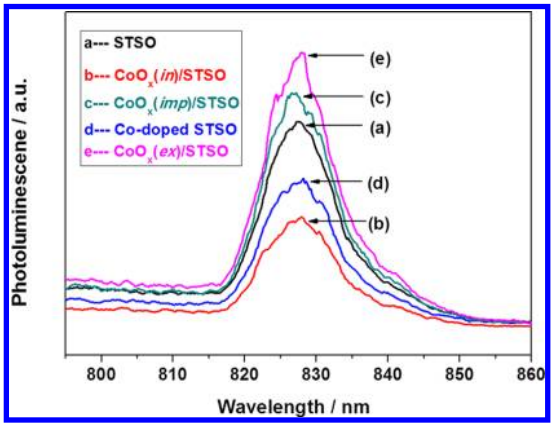

Figure 5. Photoluminescence spectra measured at 77 K with 400 nm excitation: (a) STSO; (b) $CoO_x(in)$/STSO; (c) $CoO_x(imp)$/STSO; (d) Co-doped STSO; and (e) $CoO_x(ex)$/STSO.

STSO sample generated luminescence centered at 827 nm upon excitation with 400 nm photons, similar to previous observation.[37] An obvious reduction in photoluminescence intensity without changing the maximum wavelength is observed for both Co-doped STSO and $CoO_x(in)$/STSO samples, while the PL intensities on the $CoO_x(imp)$/STSO and $CoO_x(ex)$/STSO samples are both increased. It means that the cobalt doping or *in situ* cobalt deposition can efficiently passivate the defect sites that generally act as electron−hole recombination centers, while the conventional cobalt impregnation or *ex situ* sulfurization-assisted deposition leads to increased amount of defect sites. Since partial doping of Co to substitute Ti atoms has been indicated by the above XRD results, the reduced photoluminescence intensities in both Co-doped STSO and $CoO_x(in)$/STSO samples can be ascribed to prevention of defect sites formation by the cobalt substitution. Oppositely, the increase of the PL intensities in the $CoO_x(imp)$/STSO and $CoO_x(in)$/STSO samples should originate from production of new defect sites during the calcinations and additional sulfurization process used for the cobalt deposition.

In order to further understand the influences of the cobalt doping and/or deposition on the dynamics of photogenegrated charge carries, time-resolved infrared absorption (TR-IR) measurements were conducted. The electron−hole recombination kinetics observed by TP-IR spectroscopy (Figure 6) show

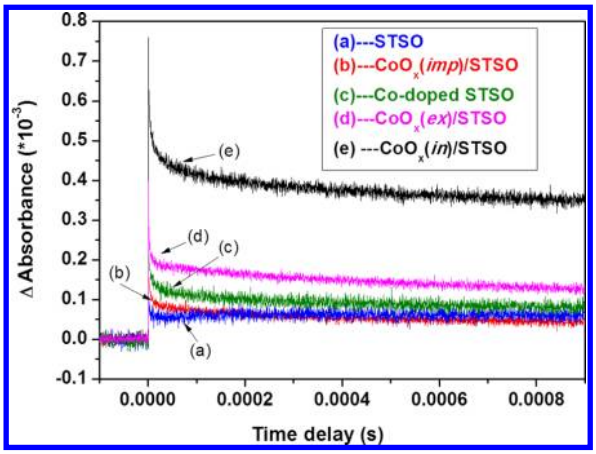

Figure 6. Time-resolved infrared absorption (TR-IR) measurements of several typical samples: (a) STSO; (b) $CoO_x(imp)$/STSO; (c) Co-doped STSO; (d) $CoO_x(ex)$/STSO; and (e) $CoO_x(in)$/STSO. The pulse laser at 355 nm (1 Hz, 3 mJ/pulse) was used to excite the samples.

that the lifetime of long-lived photogenerated electrons in the microsecond time scale for $CoO_x(in)$/STSO is much longer than other samples. The lifetimes of the exited electrons on $CoO_x(ex)$/STSO, Co-doped STSO, and $CoO_x(imp)$/STSO samples are enhanced to a different extent with respect to the parent STSO sample, and charge carriers with longer lifetime correspond to higher water oxidation activity in Table 1. Such long-lived electrons are most likely responsible for the enhancement in the photocatalytic activity.[45−47] Both CoO_x cocatalyst and cobalt doping play roles in separating the photogenerated electrons and holes, as should be responsible for the promotion of water oxidation. In this work, the *in situ* cobalt deposition not only produces CoO_x cocatalsyt as active sites but also leads to part cobalt doping to inhibit formation of Ti^{3+} ions as defect sites, so the $CoO_x(in)$/STSO photocatalyst shows the highest O_2 activity. Compared to the *in situ* cobalt deposition, the *ex situ* cobalt deposition can also create CoO_x cocatalyst for efficient separation of photogenerated carriers, but it undergoes an additional sulfurization process to form increased defect sites indicated by the PL measurement, and it shows moderate O_2 evolution activity. However, the conventional cobalt impregnation just promotes slightly the separation of carriers but causes more defect sites, so its promotion effect is the least obvious among all the cocatalysts examined.

dx.doi.org/10.1021/jp310138b | J. Phys. Chem. C 2013, 117, 376−382

CONCLUSIONS

In summary, cobalt oxide is found to be efficient cocatalyst for photocatalytic water oxidation on the $CoO_x/Sm_2Ti_2S_2O_5$ catalyst under visible light irradiation. A remarkable promotion of O_2 evolution rate is achieved and ascribed to novel deposition of cobalt cocatalyst by the sulfurization-assisted *in situ* or *ex situ* processes. The *in situ* cobalt deposition introduced in this work not only produces active CoO_x cocatalysts but also maintains the structure of photocatalyst and inhibits formation of defect sites; all of the advantages together contribute to the highest water oxidation performance among the oxysulfide photocatalysts to date. The apparent quantum efficiency is 5.0% at 420 nm, which is the highest O_2 evolution efficiency for oxysulfides reported so far. The sulfurization-assisted cobalt deposition is expected to be a promising way of loading modifiers to fabricate (oxy)sulfide-based composites.

ASSOCIATED CONTENT

Supporting Information

More experimental details on the HRTEM, XPS, Raman characterization, and the optimization of cocatalysts amount (Figures S1−S7 and Table S1). This material is available free of charge via the Internet at http://pubs.acs.org.

AUTHOR INFORMATION

Corresponding Author

*E-mail canli@dicp.ac.cn, Tel 86-411-84379070, Fax 86-411-84694447 (C.L.); e-mail domen@chemsys.t.u-tokyo.ac.jp, Tel 81-3-5841-1148, Fax 81-3-5841-8838 (K.D.).

Author Contributions

The manuscript was written through contributions of all authors. All authors have given approval to the final version of the manuscript.

Notes

The authors declare no competing financial interest.

ACKNOWLEDGMENTS

This work was financially supported by National Natural Science Foundation of China (No. 21061140361, 21090340); Solar Energy Action Plan of Chinese Academy of Sciences (ACS); Hundred Talents Program of DICP, ACS; SKLC Independent Research Projects; and 973 National Basic Research Program of the Ministry of Science and Technology (Grant 2009CB220010).

REFERENCES

(1) Graetzel, M. *Acc. Chem. Res.* **1981**, *14*, 376−384.
(2) Gust, D.; Moore, T. A.; Moore, A. L. *Acc. Chem. Res.* **2009**, *42*, 1890−1898.
(3) Meyer, T. J. *Acc. Chem. Res.* **1989**, *22*, 163−170.
(4) Bard, A. J.; Fox, M. A. *Acc. Chem. Res.* **1995**, *28*, 141−145.
(5) Barber, J. *Chem. Soc. Rev.* **2008**, *38*, 185−196.
(6) Toma, F. M.; Sartorel, A.; Iurlo, M.; Carraro, M.; Parisse, P.; Maccato, C.; Rapino, S.; Gonzalez, B. R.; Amenitsch, H.; Da Ros, T. *Nat. Chem.* **2010**, *2*, 826−831.
(7) Miseki, Y.; Kato, H.; Kudo, A. *Energy Environ. Sci.* **2009**, *2*, 306−314.
(8) Iizuka, K.; Wato, T.; Miseki, Y.; Saito, K.; Kudo, A. *J. Am. Chem. Soc.* **2011**, *133*, 20863−20868.
(9) Sato, J.; Saito, N.; Yamada, Y.; Maeda, K.; Takata, T.; Kondo, J. N.; Hara, M.; Kobayashi, H.; Domen, K.; Inoue, Y. *J. Am. Chem. Soc.* **2005**, *127*, 4150−4151.
(10) Kadowaki, H.; Saito, N.; Nishiyama, H.; Kobayashi, H.; Shimodaira, Y.; Inoue, Y. *J. Phys. Chem. C* **2007**, *111*, 439−444.
(11) Inoue, Y. *Energy Environ. Sci.* **2009**, *2*, 364−386.
(12) Maeda, K.; Abe, R.; Domen, K. *J. Phys. Chem. C* **2011**, *115*, 3057−3064.
(13) Hoertz, P. G.; Kim, Y.-I.; Youngblood, W. J.; Mallouk, T. E. *J. Phys. Chem. B* **2007**, *111*, 6845−6856.
(14) Yokoyama, D.; Hashiguchi, H.; Maeda, K.; Minegishi, T.; Takata, T.; Abe, R.; Kubota, J.; Domen, K. *Thin Solid Films* **2011**, *519*, 2087−2092.
(15) Frame, F. A.; Townsend, T. K.; Chamousis, R. L.; Sabio, E. M.; Dittrich, T.; Browning, N. D.; Osterloh, F. E. *J. Am. Chem. Soc.* **2011**, *133*, 7264−7267.
(16) Lee, Y.; Suntivich, J.; May, K. J.; Perry, E. E.; Shao-Horn, Y. *J. Phys. Chem. Lett.* **2012**, *3*, 399−404.
(17) Kanan, M. W.; Nocera, D. G. *Science* **2008**, *321*, 1072−1075.
(18) Kanan, M. W.; Surendranath, Y.; Nocera, D. G. *Chem. Soc. Rev.* **2008**, *38*, 109−114.
(19) Kanan, M. W.; Yano, J.; Surendranath, Y.; Dincă, M.; Yachandra, V. K.; Nocera, D. G. *J. Am. Chem. Soc.* **2010**, *132*, 13692−13701.
(20) El Baydi, M.; Tiwari, S. K.; Singh, R. N.; Rehspringer, J. L.; Chartier, P.; Koenig, J. F.; Poillerat, G. *J. Solid State Chem.* **1995**, *116*, 157−169.
(21) Haenen, J.; Visscher, W.; Barendrecht, E. *J. Electroanal. Chem.* **1986**, *208*, 297−321.
(22) Kamata, K.; Maeda, K.; Lu, D.; Kako, Y.; Domen, K. *Chem. Phys. Lett.* **2009**, *470*, 90−94.
(23) Zhang, F.; Yamakata, A.; Maeda, K.; Moriya, Y.; Takata, T.; Kubota, J.; Teshima, K.; Oishi, S.; Domen, K. *J. Am. Chem. Soc.* **2012**, *134*, 8348−8351.
(24) Liao, M.; Feng, J.; Luo, W.; Wang, Z.; Zhang, J.; Li, Z.; Yu, T.; Zou, Z. *Adv. Funct. Mater.* **2012**, *22*, 3066−3074.
(25) Hitoki, G.; Ishikawa, A.; Takata, T.; Kondo, J. N.; Hara, M.; Domen, K. *Chem. Lett.* **2002**, 736−737.
(26) Lu, D.; Hara, M.; Hisatomi, T.; Takata, T.; Domen, K. *J. Phys. Chem. C* **2009**, *113*, 17151−17155.
(27) Ishikawa, A.; Takata, T.; Kondo, J. N.; Hara, M.; Kobayashi, H.; Domen, K. *J. Am. Chem. Soc.* **2002**, *124*, 13547−13553.
(28) Zhang, F.; Maeda, K.; Takata, T.; Hisatomi, T.; Domen, K. *Catal. Today* **2012**, *185*, 253−258.
(29) Yamada, Y.; Ishikawa, A.; Takata, T.; Nomura, J.; Hara, M.; Domen, K. *Nippon Kagakkai Koen Yokoshu* **2003**, *83*, 169.
(30) Ishikawa, A.; Takata, T.; Matsumura, T.; Kondo, J. N.; Hara, M.; Kobayashi, H.; Domen, K. *J. Phys. Chem. B* **2004**, *108*, 2637−2642.
(31) Maeda, K.; Teramura, K.; Lu, D.; Takata, T.; Saito, N.; Inoue, Y.; Domen, K. *Nature* **2006**, *440*, 295−295.
(32) Maeda, K.; Takata, T.; Hara, M.; Saito, N.; Inoue, Y.; Kobayashi, H.; Domen, K. *J. Am. Chem. Soc.* **2005**, *127*, 8286−8287.
(33) Maeda, K.; Teramura, K.; Lu, D.; Saito, N.; Inoue, Y.; Domen, K. *Angew. Chem., Int. Ed.* **2006**, *118*, 7970−7973.
(34) Maeda, K.; Xiong, A.; Yoshinaga, T.; Ikeda, T.; Sakamoto, N.; Hisatomi, T.; Takashima, M.; Lu, D.; Kanehara, M.; Setoyama, T. *Angew. Chem., Int. Ed.* **2010**, *122*, 4190−4193.
(35) Ishikawa, A.; Yamada, Y.; Takata, T.; Kondo, J. N.; Hara, M.; Kobayashi, H.; Domen, K. *Chem. Mater.* **2003**, *15*, 4442−4446.
(36) Zhang, F.; Maeda, K.; Takata, T.; Domen, K. *Chem. Commun.* **2010**, *46*, 7313−7315.
(37) Zhang, F.; Maeda, K.; Takata, T.; Domen, K. *J. Catal.* **2011**, *280*, 1−7.
(38) Jansson, J.; Palmqvist, A. E. C.; Fridell, E.; Skoglundh, M.; Österlund, L.; Thormählen, P.; Langer, V. *J. Catal.* **2002**, *211*, 387−397.
(39) Hyman, M. P.; Vohs, J. M. *Surf. Sci.* **2011**, *605*, 383−389.
(40) Hadjiev, V.; Iliev, M.; Vergilov, I. *J. Phys. C: Solid State Phys.* **2000**, *21*, L199−L201.
(41) Kudo, A.; Omori, K.; Kato, H. *J. Am. Chem. Soc.* **1999**, *121*, 11459−11467.
(42) Hitoki, G.; Takata, T.; Kondo, J.; Hara, M.; Kobayashi, H.; Domen, K. *Chem. Commun.* **2002**, 1698−1699.

(43) Kasahara, A.; Mukumizu, K.; Hitoki, G.; Takata, T.; Kondo, J. N.; Hara, M.; Kobayashi, H.; Domen, K. *J. Phys. Chem. B* **2003**, *107*, 791−797.
(44) Kasahara, A.; Nukumizu, K.; Hitoki, G.; Takata, T.; Kondo, J. N.; Hara, M.; Kobayashi, H.; Domen, K. *J. Phys. Chem. A* **2002**, *106*, 6750−6753.
(45) Chen, T.; Feng, Z. H.; Wu, G. P.; Shi, J. Y.; Ma, G. J.; Ying, P. L.; Li, C. *J. Phys. Chem. C* **2007**, *111*, 8005−8014.
(46) Yamakata, A.; Ishibashi, T.; Onishi, H. *J. Phys. Chem. B* **2002**, *106*, 9122−9125.
(47) Thompson, T. L.; Yates, J. T. *Chem. Rev.* **2006**, *106*, 4428−4453.

NOTE ADDED AFTER ASAP PUBLICATION

This article was published ASAP on December 31, 2012. Figures 5 and 6 have been modified. The correct version was published on January 10, 2013.